Dynamical screening in strongly correlated metal $SrVO_3$

Li Huang[1,2,3] [(a)] and Yilin Wang[1,2]

[1] *Beijing National Laboratory for Condensed Matter Physics, Chinese Academy of Sciences, Beijing 100190, China*
[2] *Institute of Physics, Chinese Academy of Sciences, Beijing 100190, China*
[3] *Science and Technology on Surface Physics and Chemistry Laboratory, P.O. Box 718-35, Mianyang 621907, China*

PACS 71.27.+a – Strongly correlated electron systems; heavy fermions
PACS 71.10.-w – Theories and models of many-electron systems
PACS 71.15.-m – Methods of electronic structure calculations
PACS 71.30.+h – Metal-insulator transitions and other electronic transitions

Abstract – The consequences of dynamical screening of Coulomb interaction among correlated electrons in realistic materials have not been widely considered before. In this letter we try to incorporate a frequency dependent Coulomb interaction into the state-of-the-art *ab initio* electronic structure computing framework of local density approximation plus dynamical mean-field theory, and then choose $SrVO_3$ as a prototype material to demonstrate the importance of dynamical screening effect. It is shown to renormalise the spectral weight near the Fermi level, to increase the effective mass, and to suppress the t_{2g} quasiparticle band width apparently. The calculated results are in accordance with very recent angle-resolved photoemission spectroscopy experiments and Bose factor ansatz calculations.

Introduction. – Over the last years, tremendous progresses have been made in the investigations of strongly correlated materials. [1–3] Such systems typically contain partially filled and relatively localized $3d$, $4f$ or $5f$ orbitals, and the low-energy physics of these systems is generally described by an effective Hamiltonian which models the electronic Coulomb interaction among these correlated orbitals. The electronic Coulomb interaction can be generally parameterized by a number, the "Hubbard U". Usually U is assumed to be static, but in principle U is dynamical and frequency dependent: electric fields will be induced by the charge density fluctuation in correlated orbitals, while the higher or lower-lying states in the systems will act to screen, resulting in a frequency dependent renormalization. [4–6] On one hand, it is realized that at high frequency the screening becomes weaker and eventually the interaction approaches the large bare Coulomb value, which is an order of magnitude larger than the static screened value. On the other hand, it is generally believed that the dynamical screening effect may play a key role in understanding the subtle electronic structures of strongly correlated materials, [7–9] for examples, plasmon satellites and spectral weight transfer in photoemission spectra of hole-doped $BaFe_2As_2$. [10] Thus how to take the dynamical screening effect into consideration is one of the challenges in studying the intriguing properties of strongly correlated materials.

In a realistic approach to strongly correlated materials, the frequency dependent $U = U(\omega)$ can be evaluated at the random phase approximation (RPA) level, which allows for the direct evaluations of matrix elements of Hubbard U and its frequency dependence. [4–6] The static screened value $U_0 = \Re U(\omega = 0)$, has been widely used in the local density approximation plus static Coulomb interaction (LDA + U) method [11, 12] and local density approximation combined with dynamical mean-field theory (LDA + DMFT) approach. [1–3, 13–15] Since the frequency dependent screening has been completely neglected or empirically taken into account by adjusting the effective static U_0, very little is known on the consequences of frequency dependent Coulomb interaction in the electronic structures of strongly correlated materials. In order to include the dynamical screening effect into the LDA + DMFT framework, the hardest obstacle has been the lack of a reliable and efficient quantum impurity solver for the general impurity model with a frequency dependent Coulomb interaction $U(\omega)$. [8]

Fortunately, this obstacle has been recently overcome by the development of strong coupling continuous-time quantum Monte Carlo impurity solver (abbreviated CT-

[(a)] E-mail: lihuang@iphy.ac.cn

HYB) proposed by Werner *et al.* [8,16–18], where a multi-plasmon Lang-Firsov transformation is treated exactly in the context of a hybridization expansion algorithm for the general impurity model. By using this powerful impurity solver, Werner *et al.* have studied the plasmon satellites and large doping and temperature dependence of electronic properties in hole-doped $BaFe_2As_2$, a fascinating iron-based superconductor. They have demonstrated that the dynamical screening effect is important not only for high-energy spectral features, such as correlation satellites seen in photoemission spectroscopy, but also for the low-energy electronic structure, mass enhancements and lifetimes of hole-doped $BaFe_2As_2$. [10] As an very useful complement, the weak coupling continuous-time quantum Monte Carlo impurity solver (abbreviated CT-INT) developed by Rubtsov *et al.* [18–20] can treat generic retarded interactions as well. But the CT-INT impurity solver is limited to small dynamical screened $U(\omega)$ and not-so-large screening frequencies ω, [20] and therefore becomes prohibitively costly for realistic applications of dynamical screening interactions in multi-orbital impurity models. M. Casula *et al.* [9] proposed a dubbed Bose factor ansatz (BFA) for the Green's function of quantum impurity problem with retarded interactions, in which the Green's function is factorized into a contribution stemming from an effective static-U problem and a bosonic high-energy part introducing collective plasmon excitations. Various approximations for the Green's function Bose factor F are introduced and their pros and cons are analyzed carefully. The most practical and effective one is borrowed directly from the so-called dynamical atomic limit approximation (DALA), whose functional form is analytically known. Since the DALA is valid in the hybridization $\Delta = 0$ limit, it only works well in the intermediate-strong coupling regime, with U_0 and the dynamical part large enough. The other functional forms going beyond the DALA scheme are available as well. [9]

Inspired by Werner *et al.*'s pioneer works, [7,10] in this letter we try to incorporate the dynamical screening effect into the LDA + DMFT computing framework by adopting their approach. [8,16–18] Then we apply this technique to solve a realistic multi-band Hamiltonian with dynamical Coulomb interaction $U(\omega)$ for prototypical transition metal oxide $SrVO_3$. The quasiparticle weight reduction, more renormalized t_{2g} band width and the spectral weight transfer to higher frequencies are found and analyzed in details. Our calculations highlight the importance of including the proper screened interaction, to have a correct and reliable description of the electronic correlation in strongly correlated materials.

Method. – The computational scheme used in present work can be viewed as an extension of the traditional LDA + DMFT method. [1–3] In a Hamiltonian formulation, the multi-orbital model with dynamically screened interactions can be written as

$$H = H_{\rm LDA}^{\rm TB} - H_{\rm DC} + H_{\rm I} + H_{\rm S}. \tag{1}$$

Here $H_{\rm LDA}^{\rm TB}$ is the single particle low-energy effective Hamiltonian. To generate $H_{\rm LDA}^{\rm TB}$, the ground state calculation by using the pseudopotential plane-wave method with the ABINIT package [21] has been performed at first. For the ground state calculation, the projector augmented wave (PAW) type pseudopotentials [22] for Sr, V and O species are constructed by ourselves, the cutoff energy for plane-wave expansion is 20 Ha, and the k-mesh for Brillouin zone integration is $12\times12\times12$. These pseudopotentials and computational parameters are carefully checked and tuned to ensure the numerical convergences. And then $H_{\rm LDA}^{\rm TB}$ is obtained by applying a projection onto maximally localized Wannier function (MLWF) [23] orbitals including all the V-t_{2g} and O-$2p$ orbitals, which resulting in a 12×12 tight-binding Hamiltonian. $H_{\rm DC}$ is the double counting term, and the around mean-field (AMF) scheme [12] is used, which is especially suitable for strongly correlated metal system. The Coulomb interaction term $H_{\rm I}$ is taken into consideration merely among three V-t_{2g} orbitals. In the present work, we choose $U = 4.0$ and $J = 0.65$ eV, which are close to previous estimations. [13,15] The bosonic part $H_{\rm S}$ reads

$$H_{\rm S} = \sum_i \int {\rm d}\omega \left[\lambda_{i\omega}(b_{i\omega}^\dagger + b_{i\omega}) \sum_\alpha n_{i\alpha} + \omega b_{i\omega}^\dagger b_{i\omega} \right], \tag{2}$$

which describes the coupling of electronic degrees of freedom (occupation number n) to bosonic modes (bosonic operators $b^\dagger$ and b) and the coupling strength $\lambda_\omega = \sqrt{\Im U(\omega)/\pi}$. The bosonic modes represent the screening of the charge density fluctuations on the strongly correlated V-t_{2g} orbitals.

The multi-orbital lattice problem is studied using DMFT, [1,2] which maps it to a self-consistent solution of a three-orbital quantum impurity model. Then the impurity model (with frequency-dependent interactions $U(\omega)$) is solved using the CT-HYB impurity solver [8, 16–18] which based on a stochastic diagrammatic expansion of the partition function in the impurity-bath hybridization. In fact, the effect of $U(\omega)$ is to dress the fermionic propagators with a bosonic propagator $\exp[-\mathcal{K}(\tau)]$ where $\mathcal{K}(\tau)$ is the twice-integrated retarded interaction. In terms of $\Im U(\omega)$ and a factor $\mathcal{B}(\tau,\omega) = \cosh[(\tau-\frac{\beta}{2})\omega]/\sinh[\frac{\beta\omega}{2}]$ with bosonic symmetry, $\mathcal{K}(\tau)$ can be expressed by [8,10]

$$\mathcal{K}(\tau) = \int_0^\infty \frac{d\omega}{\pi} \frac{\Im U(\omega)}{\omega^2} [\mathcal{B}(\tau,\omega) - \mathcal{B}(0,\omega)]. \tag{3}$$

Thus the diagrammatic weight for Monte Carlo stochastic sampling is supplemented with an additional bosonic term, which originates from the contribution of $\mathcal{K}(\tau)$. The implemented details of CT-HYB impurity solver improved with recently developed orthogonal polynomial representation algorithm [24] can be easily found in the literatures. [8, 16, 17] In each LDA + DMFT iterations, typically 4×10^8 Monte Carlo samplings have been performed to reach sufficient numerical accuracy. All the calculations are carried out at the inverse temperature of $\beta = 10$

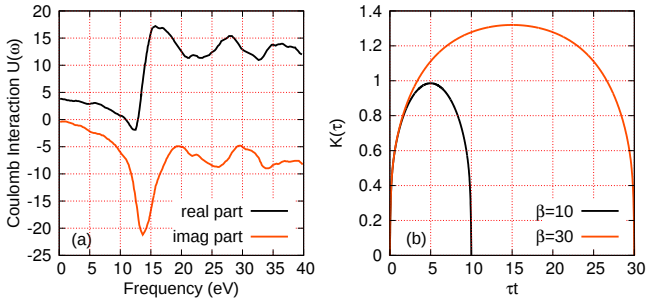

Fig. 1: (Color online) Frequency dependent interaction for $SrVO_3$ from constrained random phase approximation. (a) Real and imaginary parts of the average intra-orbital Coulomb interaction as a function of frequency. The data shown in this figure are taken from reference [5] directly. (b) The twice-integrated retarded interaction function $\mathcal{K}(\tau)$ at finite temperatures $\beta = 10$ and $\beta = 30$ calculated by Eq.(3).

or $\beta = 30$. Finally the maximum entropy method [25] is used to perform analytical continuation to obtain the impurity spectral functions of V-t_{2g} states.

Results and discussion. – $SrVO_3$ is a prototype of correlated metal and very well studied material which represents a benchmark for theories describing strongly correlated compounds. [9] Indeed, its band structure is relatively simple due to its undistorted perovskite structure, resulting in the occupation of one electron in threefold degenerate V-t_{2g} bands crossing the Fermi level. The Oxygen $2p$ bands are quite well separated from the t_{2g} levels, such that the 3×3 V-t_{2g} tight-binding Hamiltonian is a minimal model required for a correct description of the low-energy physics of $SrVO_3$. Thus, $SrVO_3$ has been the testing case for many new LDA + DMFT implementations. [13–15, 26–29] And on the other hand, $SrVO_3$ has been the subject of intensive experimental activity, with magnetic, electrical, optical measurements, and by means of angle-resolved photoemission spectroscopy (ARPES). [30–33] Therefore $SrVO_3$ is an ideal system to benchmark our newly developed implementation of LDA + DMFT computing framework incorporated with dynamical screening interaction.

To include dynamical screening interaction within LDA + DMFT computing scheme, one of the bottlenecks is the determination of the frequency dependent Coulomb interaction $U(\omega)$ and corresponding twice-integrated retarded interaction $\mathcal{K}(\tau)$. Recent works try to extract these quantities from constrained density functional calculations, [11] GW-inspired methods, [4] or RPA-based schemes. [5, 6] All these calculations are very tedious and tricky. Fortunately, the realistic frequency dependent $U(\omega)$ for $SrVO_3$ has been computed before [5] based on the constrained RPA (cRPA) approach, so we can extract $U(\omega)$ directly from the reference as a necessary input to evaluate $\mathcal{K}(\tau)$ in the preprocessing stage. The obtained $U(\omega)$ and $\mathcal{K}(\tau)$ are shown in Fig.1 respectively. Clearly seen in Fig.1(a),

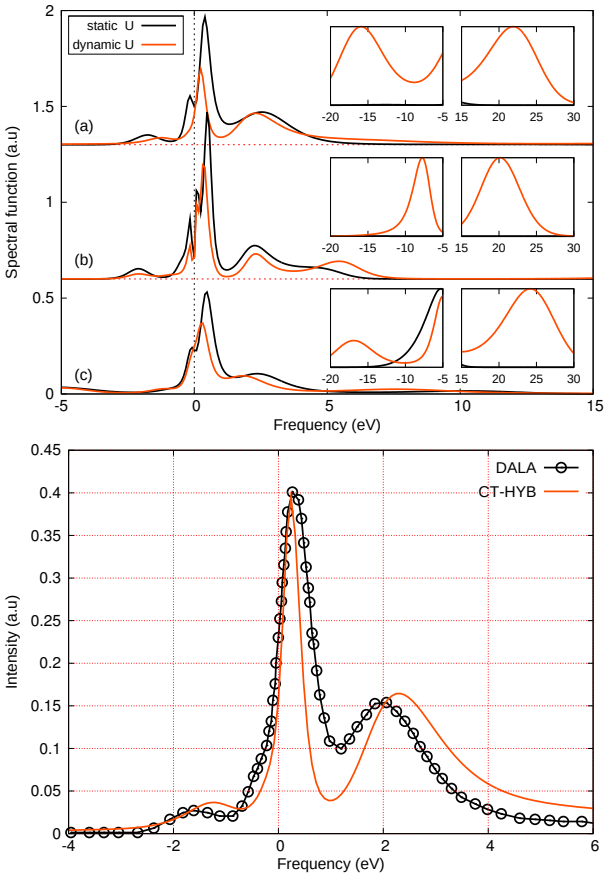

Fig. 2: (Color online) Integrated spectral functions $A(\omega)$ of V-t_{2g} states. Upper panel: Spectral functions obtained in current LDA + DMFT calculations for different models. (a) $N_{\text{wann}} = 3$, $\beta = 10$; (b) $N_{\text{wann}} = 3$, $\beta = 30$; (c) $N_{\text{wann}} = 12$, $\beta = 10$. Inset: The fine structures of spectral functions at high frequencies. The spectral functions are obtained from imaginary-time Green's functions $G(\tau)$ by using maximum entropy method, [25] and the results are cross-checked by using recently developed stochastic analytical continuation method. [34] Lower panel: Comparison of spectral functions of V-t_{2g} states obtained by our LDA + DMFT calculations with CT-HYB impurity solver and BFA-DALA method respectively. $N_{\text{wann}} = 3$, $\beta = 10$. The results obtained by BFA-DALA method are extracted directly from the reference [9].

$\Im U(\omega)$ features prominent peaks at 14 eV, 26 eV and 33 eV respectively. From the peaks of $\Im U(\omega)/\omega^2$, the energies of plasmon satellite structures in the V-t_{2g} density of states can be easily concluded. The real part of $U(\omega)$ ranges from the static screened value $U_0 = 4.0$ eV to the bare unscreened value of about 12 eV at large ω, and the frequency dependence resembles typical $U(\omega)$ in strongly correlated metals. In a standard LDA + DMFT calculation without dynamical screening effect, the relatively small value of static screened value U_0 would result in a rather weakly correlated picture.

Now let's focus on the spectral properties of V-t_{2g} states. Two different models for $SrVO_3$ are taken into

considerations, one contains only the V-t_{2g} states (number of Wannier orbitals $N_{\rm wann} = 3$), the other contains both V-t_{2g} and O-2p states (number of Wannier orbitals $N_{\rm wann} = 12$). We solve these models in the framework of LDA + DMFT at $\beta = 10$ and $\beta = 30$ with dynamical U and static U respectively. The calculated results are illustrated in the upper panel of Fig.2. The results obtained by dynamical U and static U calculations display remarkable differences. Firstly, in the dynamical U calculations, spectral weights are shifted strongly to high frequencies, which leads to a reduction in weight at low energies, compared with the static U results. Secondly, the quasiparticle resonance peak around the Fermi level is strongly renormalized, not only the width but also the height of it shrink apparently as $U(\omega)$ is taken into account. Thirdly, in dynamical U calculations, some shoulder peaks near $\omega = 0$ are smeared out. Thus, the explicit treatment of the Coulomb repulsion at large frequencies has a substantial effect, even on the low-energy properties of the system. [8–10]

We note that recently Casula *et al.* [9] have studied the spectral properties of $SrVO_3$ by using their BFA-DALA method. Since both the BFA-DALA method and our CT-HYB scheme are intent to deal with the strongly correlated systems with frequency dependent Coulomb interaction, it should be meaningful to justify the calculated results obtained by these two different methods. Comparison of the calculated spectral functions of V-t_{2g} states are shown in the lower panel of Fig.2. Both spectral functions exhibit significant three-peak structures, which are prominent for strongly correlated metal systems. [1] Clearly, the spectral function obtained by our CT-HYB scheme is consistent with that obtained by BFA-DALA method, besides a slightly spectral weight reduction near the Fermi level and a small shift of the upper Hubbard band to high energies. These discrepancies are certainly due to the smaller value of static screened U ($U_0 = 3.6$ eV) used in Casula *et al.*'s BFA-DALA calculations. [9]

In Figure 3 the calculated self-energy function of V-t_{2g} states are reported. Let's concentrate our attention to the imaginary part of self-energy function at matsubara frequency axis at first. In dynamical U model, $-\Im\Sigma(i\omega \to 0)$ is remarkable larger than that of corresponding static U model. According to the well-known Eliashberg equation: [1] $Z^{-1} \approx 1 - \frac{\beta}{\pi}\Im\Sigma(i\omega \to 0)$, the quasiparticle weight Z can be approximately evaluated. Thus the dynamical screening effect results in a smaller value of Z, namely a larger value of effective mass m^*. Indeed, for the realistic dynamical U model we found a $Z \approx 0.43 \sim 0.48$, which gives an effective mass renormalized by $2.1 \sim 2.3$ with respect to the LDA band structure. On the other hand, for the corresponding static U model we obtained a value of $Z \approx 0.6$, which underestimates the electronic correlation by a factor of 1.67, and so the value of m^*. Recent ARPES data yielded an effective mass $m^* \approx 2m_0$, [30–32] which is in good agreement with our findings for the realistic dynamical interaction. It is worthy noting that a static U

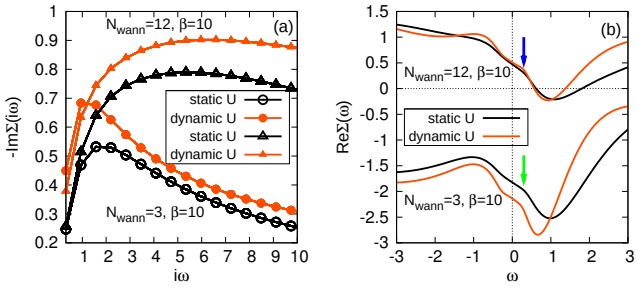

Fig. 3: (Color online) Self-energy function of V-t_{2d} states obtained by LDA + DMFT calculations at finite temperature. Left panel:Imaginary part of self-energy function at matsubara frequency axis $\Im\Sigma(i\omega)$. Right panel:Real part of self-energy function at real axis $\Re\Sigma(\omega)$. The blue and green arrows are used to indicated the "kink"-like structures, which are often considered as signatures of strongly correlated systems.

model with a larger instantaneous U_0 [26–28] can be used to fit the experimental mass renormalization artificially. But the lower Hubbard band peaked at -1.5 eV can not be obtained by such a static model. The difficulty here is to reproduce both the effective mass and the position of the lower Hubbard band by the same model. With the dynamically screened interaction model, we can describe correctly both the effective mass ($\sim 2.1m_0$) and the lower Hubbard band peaked at ~ -1.5 eV, as is seen in both Fig.3 and Fig.2.

After careful analytical continuation, self-energy function of V-t_{2g} states at real axis is obtained and plotted in Fig.3(b). For the real part of self-energy function $\Re\Sigma(\omega)$, there are two extrema at the energies $\omega \sim \pm 1.0$ eV, originating from the crossover from the central quasiparticle resonance peak to the lower and upper Hubbard bands. In the energy regime of the quasiparticle resonance peak ranging from about -0.5 eV to 0.5 eV, $\Re\Sigma(\omega)$ can be roughly described by a straight line and the slope of it can be used to evaluate the quasiparticle weight Z as well. Not surprisingly, the quasiparticle weight Z calculated with $\Re\Sigma(\omega)$ is almost identical with that calculated with $\Im\Sigma(i\omega)$. In this energy range the Landau Fermi liquid theory is valid. Strictly speaking, the Fermi liquid regime with $\Re\Sigma(\omega) \sim -\omega$ only extends from -0.2 up to 0.2 eV, which is in accord with previous LDA + DMFT calculations. [26] Next to this Fermi liquid regime, there are pronounced "kink"-like structures in $\Re\Sigma(\omega)$ around $\omega = \pm 0.25$ eV as are highlighted by colourful arrows. Apparently, the "kink"-like structures are enhanced by the dynamical screening effects. These "kink"-like structures can be regarded as a fingerprint of strongly correlated systems [35] and become important in the context of quasiparticle dispersion and electronic specific heat. In previous LDA + DMFT calculation [26] and ARPES experiment [30] the "kink"-like structures in $SrVO_3$ have been already confirmed.

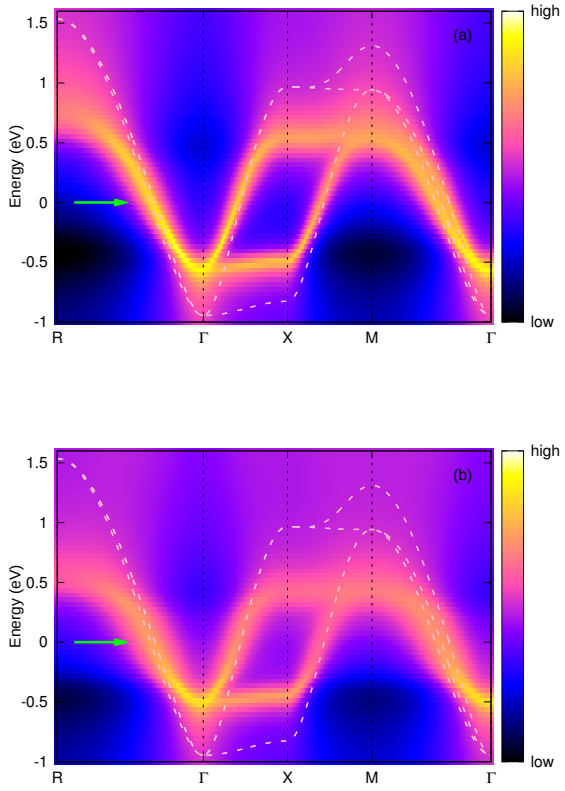

Fig. 4: (Color online) Angle-resolved spectral functions $A(\mathrm{k},\omega)$ for $SrVO_3$. Upper panel: Static Coulomb interaction case. Lower panel: Frequency dependent Coulomb interaction case. The colourful dash lines denote LDA band structures and the green arrows indicate "kink"-like structures. In these LDA + DMFT calculations, only three V-t_{2g} bands are taken into considerations and the inverse temperature β is fixed to 10.

With the knowledge of self-energy function on the real axis, we are now in the position to calculate k-resolved spectral functions or quasiparticle dispersion $A(\mathrm{k},\omega)$. The LDA + DMFT quasiparticle dispersions for dynamical U and static U models along high symmetry lines in the Brillouin zone are shown in Fig.4 respectively. The LDA band structure is presented in this figure as an useful comparison. As for the static U model, the quasiparticle band structure displays strongly band renormalization with a factor ~ 1.7 with respect to LDA band dispersion. For example, we can see from the upper panel of Fig.4 that the bottom of the quasiparticle band is located at approximately $\omega = -0.6$ eV, in contrast to the LDA value of $\omega = -1.0$ eV. Near the Fermi level along $R-\Gamma$ and $M-\Gamma$ lines there exist discernible "kink"-like structures as indicated by a green arrow, [26, 30] which stem from the shoulders in the real part of the self-energy function (see Fig.3(b)). As for the dynamical U model, its quasiparticle band structure exhibits similar features with respect to that of static U model. Around the Fermi level, the quasiparticle band structure of dynamical U model is more renormalized with a factor ~ 2.1 and has less intensity, and the bottom of quasiparticle dispersion is located at $\omega = -0.5$ eV. The "kink" structures in quasiparticle band structure are more discernible than those of corresponding static U model.

Conclusion. – In this letter, we try to incorporate the dynamical screening effect into the modern LDA + DMFT computing framework with CT-HYB as a quantum impurity solver. We apply this calculation scheme to reinvestigate the electronic structure of $SrVO_3$ with dynamical U model. It seems that the dynamical screening effect will enhance the electron correlation significantly. The transfer of spectral weight to higher frequencies, further reduction of quasiparticle resonance peak, smaller quaisparticle weight Z, larger effective mass m^*, more apparent "kink"-like structures etc. are predicted or verified by our calculations as well. Based on the calculated results, it is suggested that the dynamical screening interaction may play an important role in understanding the fine electronic structures of strongly correlated materials, which has been ignored by most of previous theoretical calculations.

* * *

We acknowledge financial support from the National Science Foundation of China and that from the 973 program of China under Contract No.2007CB925000 and No.2011CBA00108. All the LDA + DMFT calculations have been performed on the SHENTENG7000 at Supercomputing Center of Chinese Academy of Sciences (SCCAS).

REFERENCES

[1] Georges A., Kotliar G., Krauth W. and Rozenberg M. J., *Rev. Mod. Phys.*, **68** (1996) 13.
[2] Kotliar G., Savrasov S. Y., Haule K., Oudovenko V. S., Parcollet O. and Marianetti C. A., *Rev. Mod. Phys.*, **78** (2006) 865.
[3] Anisimov V. and Izyumov Y., *Electronic Structure of Strongly Correlated Materials* Vol. 163 of *Springer Series in Solid-State Sciences* (Cambridge University Press, College Station, Texas) 2012.
[4] Aryasetiawan F. and Gunnarsson O., *Rep. Prog. Phys.*, **61** (1998) 237.
[5] Aryasetiawan F., Karlsson K., Jepsen O. and Schönberger U., *Phys. Rev. B*, **74** (2006) 125106.
[6] Aryasetiawan F., Imada M., Georges A., Kotliar G., Biermann S. and Lichtenstein A. I., *Phys. Rev. B*, **70** (2004) 195104.
[7] Casula M., Werner P., Vaugier L., Aryasetiawan F., Millis A. and Biermann S., *arXiv:cond-mat/1204.4900*, (2012) .
[8] Werner P. and Millis A. J., *Phys. Rev. Lett.*, **104** (2010) 146401.
[9] Casula M., Rubtsov A. and Biermann S., *arXiv:cond-mat/1107.3123*, (2011) .

[10] Werner P., Casula M., Miyake T., Aryasetiawan F., Millis A. J. and Biermann S., *Nat. Phys.*, **8** (2012) 331337.
[11] Anisimov V. I., Zaanen J. and Andersen O. K., *Phys. Rev. B*, **44** (1991) 943.
[12] Amadon B., Jollet F. and Torrent M., *Phys. Rev. B*, **77** (2008) 155104.
[13] Amadon B., Lechermann F., Georges A., Jollet F., Wehling T. O. and Lichtenstein A. I., *Phys. Rev. B*, **77** (2008) 205112.
[14] Held K., Andersen O. K., Feldbacher M., Yamasaki A. and Yang Y.-F., *J. Phys.: Condens. Matter*, **20** (2008) 064202.
[15] Lechermann F., Georges A., Poteryaev A., Biermann S., Posternak M., Yamasaki A. and Andersen O. K., *Phys. Rev. B*, **74** (2006) 125120.
[16] Werner P., Comanac A., de' Medici L., Troyer M. and Millis A. J., *Phys. Rev. Lett.*, **97** (2006) 076405.
[17] Werner P. and Millis A. J., *Phys. Rev. Lett.*, **99** (2007) 146404.
[18] Gull E., Millis A. J., Lichtenstein A. I., Rubtsov A. N., Troyer M. and Werner P., *Rev. Mod. Phys.*, **83** (2011) 349.
[19] Rubtsov A. N., Savkin V. V. and Lichtenstein A. I., *Phys. Rev. B*, **72** (2005) 035122.
[20] Assaad F. F. and Lang T. C., *Phys. Rev. B*, **76** (2007) 035116.
[21] Gonze X., Amadon B., Anglade P.-M., Beuken J.-M., Bottin F., Boulanger P., Bruneval F., Caliste D., Caracas R., Cote M., Deutsch T., Genovese L., Ghosez P., Giantomassi M., Goedecker S., Hamann D., Hermet P., Jollet F., Jomard G., Leroux S., Mancini M., Mazevet S., Oliveira M., Onida G., Pouillon Y., Rangel T., Rignanese G.-M., Sangalli D., Shaltaf R., Torrent M., Verstraete M., Zerah G. and Zwanziger J., *Comput. Phys. Comm.*, **180** (2009) 2582.
[22] Blöchl P. E., *Phys. Rev. B*, **50** (1994) 17953.
[23] Marzari N. and Vanderbilt D., *Phys. Rev. B*, **56** (1997) 12847.
[24] Boehnke L., Hafermann H., Ferrero M., Lechermann F. and Parcollet O., *Phys. Rev. B*, **84** (2011) 075145.
[25] Jarrell M. and Gubernatis J., *Phys. Rep.*, **269** (1996) 133 .
[26] Nekrasov I. A., Held K., Keller G., Kondakov D. E., Pruschke T., Kollar M., Andersen O. K., Anisimov V. I. and Vollhardt D., *Phys. Rev. B*, **73** (2006) 155112.
[27] Pavarini E., Biermann S., Poteryaev A., Lichtenstein A. I., Georges A. and Andersen O. K., *Phys. Rev. Lett.*, **92** (2004) 176403.
[28] Nekrasov I. A., Keller G., Kondakov D. E., Kozhevnikov A. V., Pruschke T., Held K., Vollhardt D. and Anisimov V. I., *Phys. Rev. B*, **72** (2005) 155106.
[29] Lee H., Foyevtsova K., Ferber J., Aichhorn M., Jeschke H. O. and ValentíR., *Phys. Rev. B*, **85** (2012) 165103.
[30] Yoshida T., Tanaka K., Yagi H., Ino A., Eisaki H., Fujimori A. and Shen Z.-X., *Phys. Rev. Lett.*, **95** (2005) 146404.
[31] Yoshida T., Hashimoto M., Takizawa T., Fujimori A., Kubota M., Ono K. and Eisaki H., *Phys. Rev. B*, **82** (2010) 085119.
[32] Eguchi R., Kiss T., Tsuda S., Shimojima T., Mizokami T., Yokoya T., Chainani A., Shin S., Inoue I. H., Togashi T., Watanabe S., Zhang C. Q., Chen C. T., Arita M., Shimada K., Namatame H. and Taniguchi M., *Phys. Rev. Lett.*, **96** (2006) 076402.
[33] Sekiyama A., Fujiwara H., Imada S., Suga S., Eisaki H., Uchida S. I., Takegahara K., Harima H., Saitoh Y., Nekrasov I. A., Keller G., Kondakov D. E., Kozhevnikov A. V., Pruschke T., Held K., Vollhardt D. and Anisimov V. I., *Phys. Rev. Lett.*, **93** (2004) 156402.
[34] Beach K. S. D., *arXiv:cond-mat/0403055*, (2004) .
[35] Byczuk K., Kollar M., Held K., Yang Y. F., Nekrasov I. A., Pruschke T. and Vollhardt D., *Nat. Phys.*, **3** (2007) 168.